



Gas Separation Hot Paper



One-step Ethylene Purification from an Acetylene/Ethylene/Ethane Ternary Mixture by Cyclopentadiene Cobalt-Functionalized Metal–Organic Frameworks

Yutong Wang, Chunlian Hao, Weidong Fan, Mingyue Fu, Xiaokang Wang, Zhikun Wang, Lei Zhu, Yue Li, Xiaoqing Lu, Fangna Dai, Zixi Kang, Rongming Wang, Wenyue Guo, Songqing Hu, and Daofeng Sun*

Abstract: The separation of ethylene (C_2H_4) from a mixture of ethane (C_2H_6), ethylene (C_2H_4), and acetylene (C_2H_2) at normal temperature and pressure is a significant challenge. The sieving effect of pores is powerless due to the similar molecular size and kinetic diameter of these molecules. We report a new modification method based on a stable *ftw* topological Zr-MOF platform (**MOF-525**). Introduction of a cyclopentadiene cobalt functional group led to new *ftw*-type MOFs materials (**UPC-612** and **UPC-613**), which increase the host-guest interaction and achieve efficient ethylene purification from the mixture of hydrocarbon gases. The high performance of **UPC-612** and **UPC-613** for $C_2H_2/C_2H_4/C_2H_6$ separation has been verified by gas sorption isotherms, density functional theory (DFT), and experimentally determined breakthrough curves. This work provides a one-step separation of the ternary gas mixture and can further serve as a blueprint for the design and construction of function-oriented porous structures for such applications.

Introduction

Ethylene, the core of the petrochemical industry is an important chemical with which to measure the national level of a petrochemical industry.^[1,2] Three main methods to produce ethylene are ethane cracking, naphtha cracking, and light diesel cracking.^[3] Among these, naphtha cracking is currently the most industrialized but its products contain many impurities, including H_2 , CH_4 , C_2H_2 , C_2H_6 , and C_3H_6 .^[4] It is relatively easy to separate light hydrocarbons with different carbon numbers^[5–8] but the separation of C_2 gases is the most difficult, because of the very similar molecular sizes and boiling points of C_2H_2 , C_2H_4 , and C_2H_6 . At present, the common separation method is removal of ethane by cryogenic and high-pressure technology, then removal of acety-

How to cite: *Angew. Chem. Int. Ed.* **2021**, *60*, 11350–11358
International Edition: doi.org/10.1002/anie.202100782
German Edition: doi.org/10.1002/ange.202100782

lene by catalytic hydrogenation or solvent extraction, finally obtaining polymerized grade C_2H_4 through a distillation tower.^[9] This requires a large-scale separation tower, consumes much energy, accounting for about 0.3% of the global energy consumption.^[10] Consequently, it is necessary to develop a new separation method or improve the separation efficiency to achieve removal of C_2H_2 and C_2H_6 from the ternary mixture of C_2H_2 , C_2H_4 , and C_2H_6 in a single step, and obtaining the polymerized grade C_2H_4 .

Metal-organic frameworks (MOFs) with their controllable pore size and modifiable pore environment have been developed as environmentally acceptable, energy-saving and efficient gas separation materials. Many experiments have confirmed that MOFs as adsorbents can effectively separate C_2H_2/C_2H_4 , C_2H_4/C_2H_6 , C_2H_4/C_3H_6 and C_3H_6/C_3H_8 mixtures.^[11–15] Current research suggests that purification of ethylene with MOFs involves two strategies: (1) Precise control of the pore size to achieve a molecular sieving effect; (2) Selective increase of the interaction between the MOF and light hydrocarbon gases to enhance the host-guest interaction. For example, Chen et al.^[16] used a rigid square acid and calcium nitrate to limit the pore size to 3.8 Å, which caused C_2H_6 to be the first to elute through the bed from C_2H_4/C_2H_6 . It is more difficult to control the pore size precisely than to modify the host-guest interaction. Long et al.^[17] used exposed metal sites to adsorb C_2H_4 from C_2H_4/C_2H_6 thus achieving the separation of mixed gases. Practically, an industrial separation process is more useful if C_2H_4 can breakthrough first. Li et al.^[18] found that the introduction of iron(III)-peroxo sites into $Fe_2(\text{dobdc})$ (dobdc^{4-} : 2,5-dioxido-1,4-benzenedicarboxylate) would provide it with ultra-high adsorption capacity for ethane and thus preferential access to C_2H_4 . For C_2H_2/C_2H_4 mixtures, efficient separation also depends on host-guest interactions. By introducing inorganic anions with their strong hydrogen bonding capabilities into a framework, Xing et al.^[19] enhanced the specific identification of acetylene molecules and realized the efficient separation of ethylene and acetylene.

Such separation processes in industrial production are multicomponent and Zaworotko et al.^[20] mixed three kinds of adsorbents to separate and purify ethylene from the quaternary ($CO_2/C_2H_2/C_2H_6/C_2H_4$) mixtures. It is however very important, but challenging to find a single adsorption material that can achieve multi-component gas separation. While Hao et al.^[21] reported a new material, **TJT-100**, which has a strong

[*] Y. T. Wang, C. L. Hao, Dr. W. D. Fan, M. Y. Fu, X. K. Wang, Dr. Z. K. Wang, Dr. L. Zhu, Y. Li, Prof. X. Q. Lu, Prof. F. N. Dai, Z. X. Kang, Prof. R. M. Wang, Prof. W. Y. Guo, Prof. S. Q. Hu, Prof. D. F. Sun
School of Materials Science and Engineering, College of Science, China University of Petroleum (East China)
Qingdao, Shandong 266580 (China)
E-mail: dfsun@upc.edu.cn

Supporting information and the ORCID identification number(s) for the author(s) of this article can be found under:
<https://doi.org/10.1002/anie.202100782>.

interaction with C_2H_2 and C_2H_6 , thus realizing the separation of C_2H_4 from the ternary gas mixture of $C_2H_2/C_2H_6/C_2H_4$, there has been no systematic study on the selective adsorption of C_2H_2 and C_2H_6 by a single adsorbent through a pore environment modification. Moreover, stability is another important factor that realizes the industrialization of MOF materials. Hence, it remains a challenge to discover a single material with high stability which can achieve ethylene purification in one-step from multi-component gases.

In this work, we sought to develop a new method of pore environment modification based on the stable *ftw* topological Zr-MOF platform (**MOF-525**) to achieve efficient purification of C_2H_4 from $C_2H_2/C_2H_6/C_2H_4$ mixtures at room temperature and atmospheric pressure. To this end, we introduced cyclopentadiene-cobalt group into the **H₄L-L** and **H₄L-S** linker in an effort to enhance and increase the host-guest interactions. Through modular synthesis, two new functionalized Zr-MOFs, **UPC-612** and **UPC-613** with *ftw* topology were obtained (Figure 1a). Adsorption tests show that the adsorption capacities of **UPC-612** for C_2H_2 and C_2H_6 are larger than for C_2H_4 . The adsorption enthalpy (Q_{st}) at zero coverage is C_2H_2 (23.9 kJ mol^{-1}) > C_2H_6 (22.4 kJ mol^{-1}) > C_2H_4 (16.9 kJ mol^{-1}), indicating that the modified **UPC-612** has a stronger interaction with C_2H_2 and C_2H_6 than with C_2H_4 . **UPC-612** differs from **MOF-525** and **MOF-525(Co)** modified only by cobalt ions. It was shown experimentally that modified **UPC-612** can produce >99.99% pure C_2H_4 from the mixtures of C_2H_2/C_2H_4 (50/50), C_2H_6/C_2H_4 (50/50) and $C_2H_2/C_2H_6/C_2H_4$ (1/1/1). The C_2H_4 productivity of **UPC-612** from $C_2H_2/C_2H_6/C_2H_4$ (1/1/1) reaches 0.47 mmol g^{-1} , which is a new published record. Density functional theory (DFT) calculations from first principles reveal that the important adsorption sites are mainly on the corners of the cube cages and in the cyclopentadiene ring of linkers. A modified material, **UPC-613** has a similar separation effect, even though the cage diameter is reduced, and this further confirms the success of our new modification strategy in improving the separation performance of multicomponent mixture gases.

Results and Discussion

Design and Synthesis

With their high thermal and chemical stability, Zr-MOFs are promising candidates for gas separation.^[22–24] In particular, the **MOF-525** reported by Yaghi et al. is a three-dimensional *ftw* topological structure with a (4,12)-connected net, constructed with a stable Zr_6 cluster and a rigid tetracarboxyphenyl porphyrin (TCPP) network (Figure 1a).^[25] A 12-connected Zr_6 cluster has all coordination sites of the metal clusters occupied by carboxylate group, which, according to soft and hard acid-base theory^[26] improves its structural stability. In this framework, there are irregular cubes surrounded by six linkers (cubic cages, Figure 1a), and the diameter of the cage can reach about 2 nm, which can allow modifications. With a single cage as an example, the metal cluster is placed at the vertex position, and the linker acts as the face (Figure 2d). Distinct from a pore structure, in which

the guest molecules pass through the cage, they must enter through the cage window. They then make irregular movements in the cavity, finally leaving through another cage window. Therefore, the cage can be modified to increase the force between the framework and the C_2H_2 and C_2H_6 . The traditional modification methods are to expose the metal sites, for example by removal of the coordinated solvent by activation^[27,28] or to directly introduce the metal sites into the linker.^[29] It is relatively simple to introduce metal ions into the porphyrin center (Figure 2b), but the disadvantage is that this significantly enhances the effect on C_2H_4 .^[30] It has been shown that C_2H_6 can be stabilized in the pores through intermolecular dipolar and supramolecular interactions with the aromatic ligands.^[31–33] Herein, we describe a new modification, introduction of cyclopentadiene cobalt into the linker based on the stable *ftw* topology platform (Figure 1b and 2c), together with a layer of cyclopentadiene wrapped on the outer side of cobalt to selectively increase the force associated with C_2H_2 and C_2H_6 . On one hand, cyclopentadiene-cobalt can increase the weak interaction with C_2H_2 and C_2H_6 and on the other hand, it can further divide the space in the cage to form a sphere-like force surface (Figure 2f). This provides the possibility of one-step purification of C_2H_4 by the selective and exclusive adsorption of C_2H_2 and C_2H_6 .

It is necessary to compare the modification methods with the same cage diameter and to further verify the feasibility of the modification method by changing the cage diameter. Consequently, **TCPP-Co** was prepared by cobalt addition to **TCPP** as a template. **H₄L-L** and **H₄L-S** modified with cyclopentadiene cobalt were also obtained. The linker sizes of **TCPP**, **TCPP-Co**, **H₄L-L**, and **H₄L-S** were found to be 13.2 Å, 13.2 Å, 15.3 Å, and 9.5 Å, respectively. The specific synthesis steps of ligands are detailed in Figure S1–S12 in the SI.

The reaction of **H₄L-L** and $ZrCl_4$ in the presence of benzoic acid for 48 h yielded **UPC-612** as large pink crystals with cubic morphology (Figure S13). Single crystal X-ray diffraction (SC-XRD) analysis shows that **UPC-612** crystallizes in the cubic space group $Pm\bar{3}m$ (Table S1). Crystallographically, it contains a 12-connected Zr_6 cluster [$Zr_6(\mu_3-OH)_4(\mu_2-O)_4(O_2C^-)_{12}$] and a functional tetracarboxylic linker. The structure and topology are the same as in the template **MOF-525** (Figure 1). The functionalization of linkers reduced the size of the cage to 14.8 Å, and functional cyclopentadiene cobalt is introduced only on one side. During the process of self-assembly, it is uncertain in which cage each cyclopentadiene cobalt group is located. The modified functional groups showed extreme disorder in the single-crystal data. Clear pore size is important for the analysis of gas adsorption and separation. Speculation is that there can be seven different cage structures in **UPC-612**, as shown in Figure S17. According to the nitrogen adsorption at 77 K, the distribution of pore size in **UPC-612** is calculated to be 1.4 nm and 2.0 nm (Figure S15), corresponding to 6 and 0 functional groups in the cubic cage. As shown in Figure 3, the inner space of a cubic cage with six functional groups can be divided into two regions by filling the cage with a solid. A sphere-like force surface was formed by cyclopentadiene in the cage of **UPC-612** (Figure 2f and 3d). Here we compare the nearly over-

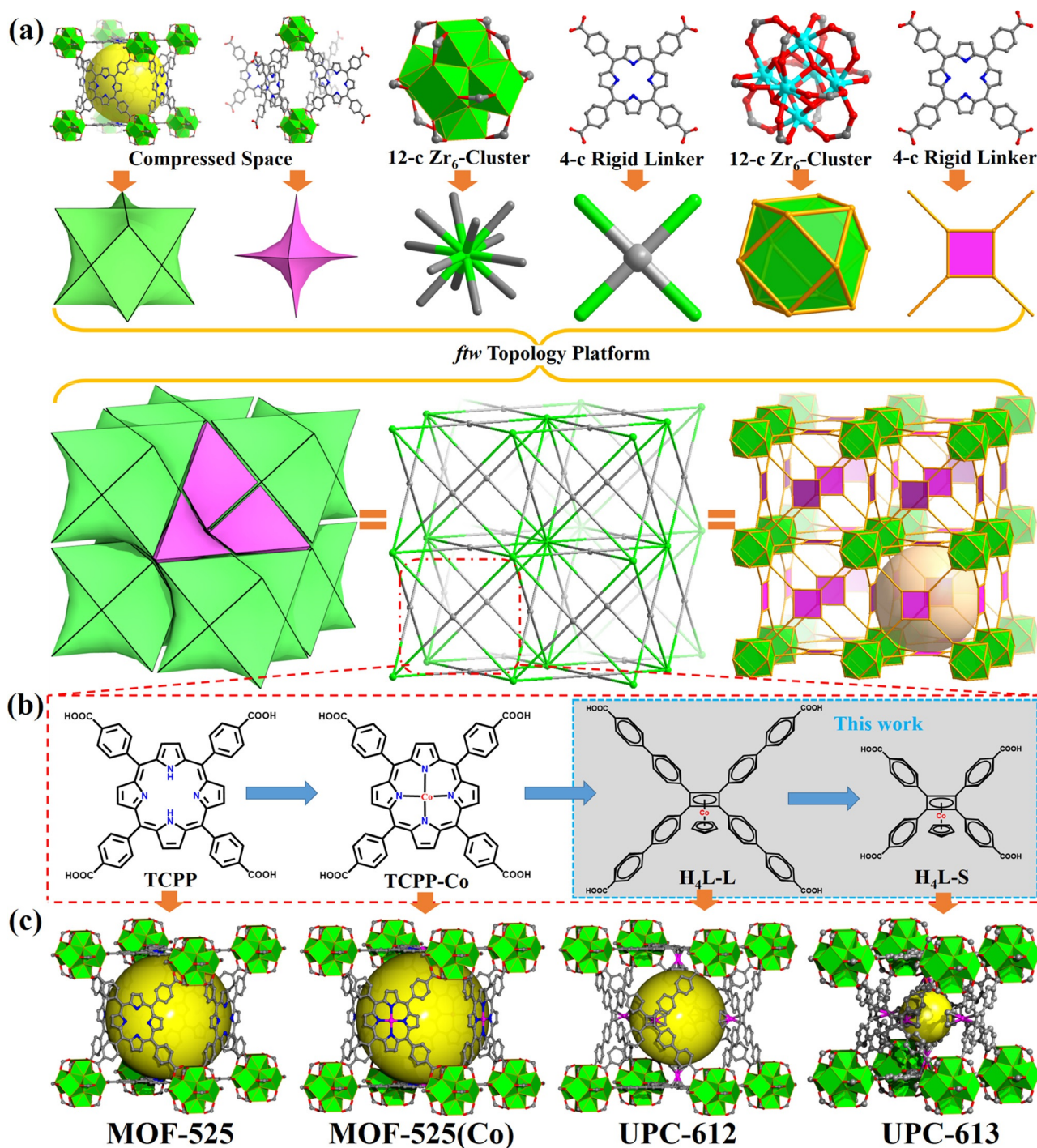


Figure 1. Illustration of *ftw* topology platform in Zr-MOFs based on different linkers: a) The interpretation of *ftw* topology from compressed space, the node, and the polyhedron; b) The progressive process of linker modification; c) Three-dimensional view of unit cubic cages assembled by different linkers. The yellow sphere indicates the available pore space.

lapping electron cloud to a spherical force surface (Figure S18).

To verify the new modification method, we introduced the same functional group into a smaller isomorphous ligand. **H₄L-S** with a size of 9.5 Å was obtained by the method similar to that used for **H₄L-L** and then assembled with a Zr₆ cluster to obtain the framework material, **UPC-613** with a smaller cage size and *ftw* topology, which exhibits a structure similar to that of **UPC-612** but with a cage diameter reduced to 7.2 and

15.7 Å. The pore size of **UPC-613** is calculated to be 0.7 nm and 1.2 nm by the nitrogen adsorption isotherm at 77 K (Figure S16). The feasibility of the new method is further verified by the control variable method, where the effect of modification group on separation performance can be determined by comparing **UPC-612** with **MOF-525**, and the effect on cage size is determined by comparing **UPC-612** with **UPC-613**.

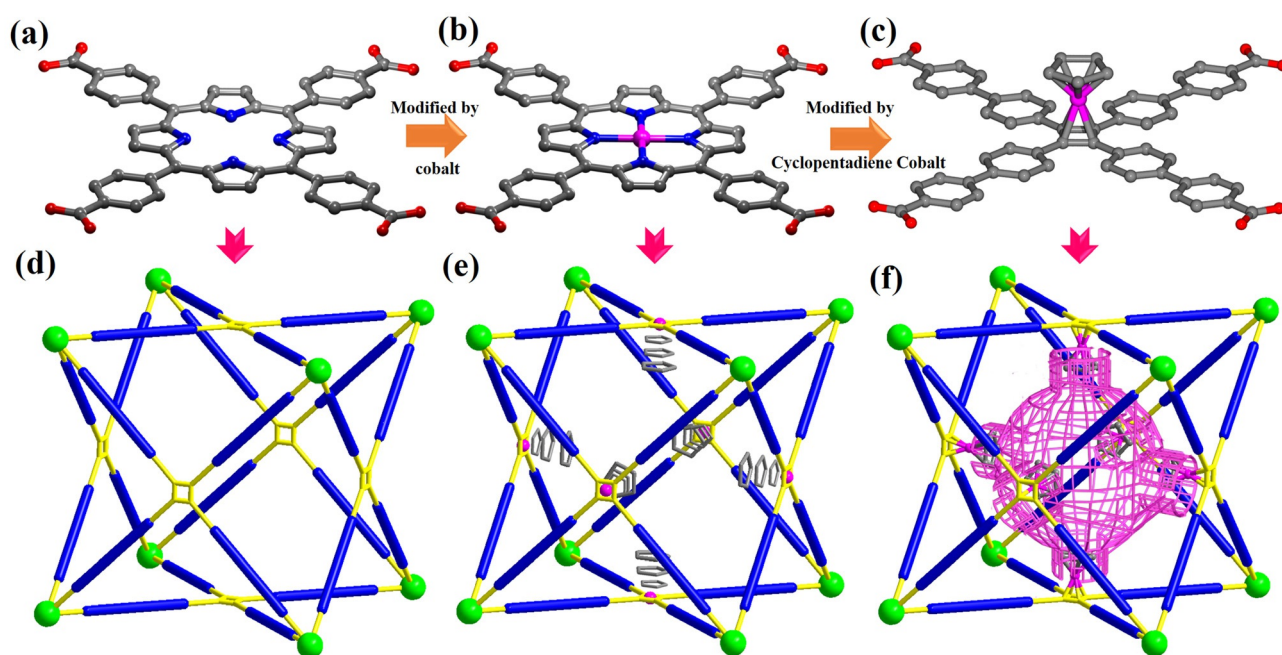


Figure 2. Design of the modification method. a) Unmodified TCPP template; b) TCPP modified by cobalt (TCPP-Co); c) Modified cyclopentadiene cobalt; d) Schematic of MOF-525 single cubic cage; e) Schematic of the force in the cage after MOF-525 is modified with metals; f) Schematic of sphere like force surface formed by the modification of cyclopentadiene cobalt.

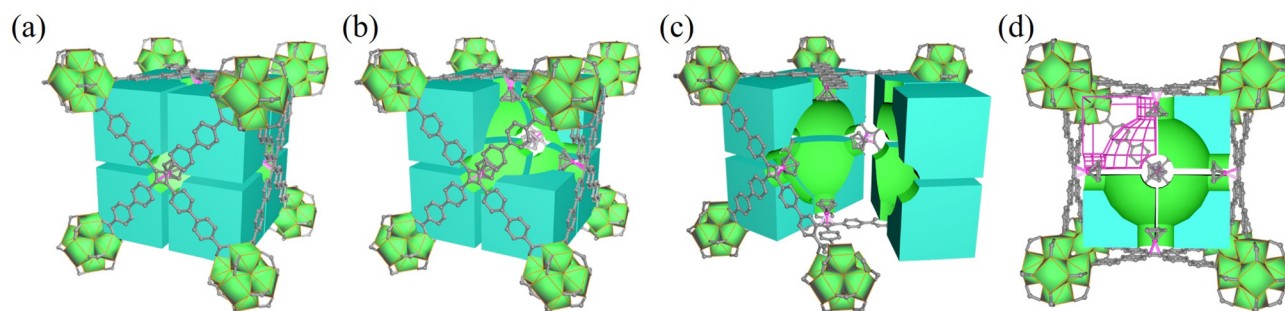


Figure 3. Structural illustration of UPC-612 with cage filling. a) Cubic cage filling of a basic unit in UPC-612; b) Space division of cubic cage; c) Internal space allocation of UPC-612 after partition; d) Cubic cage filling profile and a sphere like force surface.

Stability Studies

Stability, especially thermal and chemical stability, is a prerequisite for materials. The PXRD patterns show that both UPC-612 and UPC-613 have excellent stability due to the retained crystallinity after the breakthrough experiment (Figure S31–S33). Even if the crystal is immersed in an aqueous solution with pH values of 1–12 for 24 hours, it still maintains a good crystallinity (Figure S34,35). The thermal stability of UPC-612 and UPC-613 was measured by thermogravimetric analysis (TGA, Figure S38,S39). The initial weight loss before reaching 120 °C is attributed to the removal of the solvent molecules in the cage. The decomposition of UPC-612 and UPC-613 begins at 350 °C, and leads to the removal of organic linkers and structural collapse (Figure S36,37).

Gas Sorption

The UPC-612 and UPC-613 crystals were solvent-exchanged with dry DMF to remove the benzoic acid template from the cage. The samples were then equilibrated three times each with chromatography grade methanol and dichloromethane for 8 h. The samples were then degassed at 298 K for 12 h and then at 373 K for 10 h, until the outgas rate was 5 mm Hg min⁻¹, to produce the activated UPC-612 and UPC-613. The N₂ gas sorption curves of UPC-612 and UPC-613 at 77 K indicate their permanent porosities. UPC-612 and UPC-613 show a typical type I N₂ adsorption isotherm with a Brunauer-Emmett-Teller (BET) surface area of 2016 m² g⁻¹ for UPC-612 and 853 m² g⁻¹ for UPC-613.

Compared with MOF-525, the BET specific surface area of UPC-612 is slightly decreased. The BET specific surface area decreased from 3116 m² g⁻¹ to 2016 m² g⁻¹, which is consistent with the structure. The results show that the

modification of functional groups in the cage with the same size reduced the cage space.^[34,35] Pore size distributions were determined by nonlocal DFT calculations based on the N₂ adsorption isotherms. The pore sizes of **UPC-612** are mainly distributed between 1.5 and 2.0 nm, which is consistent with the crystallographic data.

Measurements of the C₂H₂, C₂H₄, and C₂H₆ gas adsorption capacities of activated **UPC-612** were performed. For comparison, the adsorption isotherms of **MOF-525** and **MOF-525(Co)** were also measured. The single-component adsorption isotherms of C₂H₂, C₂H₄, and C₂H₆ up to 1 atm were measured at 273, 283 and 298 K, respectively (Figure S19,20 and Table S3). As expected, the amount of adsorbed gas in **UPC-612** decreased with increasing temperature. In addition, the adsorption capacity of **UPC-612** for C₂H₄ is lower than those for C₂H₂ and C₂H₆ at two temperatures (Figure S20e,S20f), implying the distinct binding affinity of **UPC-612** for C₂H₂ and C₂H₆. At room temperature, the adsorption capacities of **UPC-612** are 67.44, 62.58, and 80.11 cm³g⁻¹ for C₂H₂, C₂H₄ and C₂H₆, respectively (Tables S3), dramatically higher than those of **MOF-525** (59.3, 47.3, and 60.7 cm³g⁻¹) and **MOF-525(Co)** (58.7, 42.9, and 49.7 cm³g⁻¹). Compared with **UPC-612**, the adsorption capacities of **UPC-613** with reduced cage diameter for C₂H₂, C₂H₄, and C₂H₆ decreased to 63.4, 51.7, and 57.1 cm³g⁻¹, respectively but are still higher than **MOF-525** and **MOF-525(Co)** with unmodified large cage diameters. This indicates that the overall adsorption capacity of C₂ gas is enhanced after modification, but the adsorption trend remains the same. At a given cage size, a higher adsorption amount represents stronger interaction, while **UPC-613** with a smaller size still shows higher adsorption capacity, which further proves the effect of the modification. Generally, a large adsorption capacity is a prerequisite for good separation ability of materials.

Reusability of porous materials is an essential condition for industrial applications. Ten adsorption-desorption cycles of **UPC-612** and **UPC-613** for C₂H₂, C₂H₄, and C₂H₆ were recorded without reactivation prior to each cycle. There was only 2.5%, 3.4%, and 2.8% loss in adsorption capacities of C₂H₂, C₂H₄, and C₂H₆ after ten cycles for **UPC-612** (Figure S21).

It is well-known that the magnitude of the adsorption enthalpies of porous materials reveals the affinity of the pore surface toward adsorbates and determines the adsorptive selectivity. To evaluate the affinity of C₂ hydrocarbons with **MOF-525**, **MOF-525(Co)**, **UPC-612** and **UPC-613**, the adsorption enthalpy (Q_{st}) for different C₂ hydrocarbons was calculated using the Clausius-Clapeyron equation. The Q_{st} values of C₂H₂, C₂H₄, and C₂H₆ are 15.81, 16.74, and 19.95 kJ mol⁻¹ in **MOF-525**, 18.57, 23.35, and 20.73 kJ mol⁻¹ in **MOF-525(Co)**, 23.94, 16.94, and 22.39 kJ mol⁻¹ in **UPC-612**, and 30.38, 28.51, and 31.83 kJ mol⁻¹ in **UPC-613** at zero coverage, respectively (Figure S22,S23 and Table S4). The results of these calculations show that **MOF-525** has the strongest affinity for C₂H₆, and is followed by C₂H₄ and finally, C₂H₂. The Q_{st} values of C₂H₄ and C₂H₆ in **MOF-525(Co)**, modified by cobalt ions were significantly increased. The modified **UPC-612** has an overall increased affinity for

C₂H₂, C₂H₄ and C₂H₆, and the affinity for C₂H₄ is the lowest. As shown in Figure S23b, a similar trend of the affinity with the order of C₂H₆ > C₂H₂ > C₂H₄ is provided by **UPC-613**. The results show that the affinity of cyclopentadiene cobalt to C₂H₆ and C₂H₂ is higher than to C₂H₄, which is useful in the separation and purification of C₂H₄. This is different from many adsorbents (Table S10). Theoretically, C₂H₂ and C₂H₆ are preferentially adsorbed from the gas mixture, while C₂H₄ can pass through the separation material successfully, and thus the purified ethylene can be obtained from the mixed gas in a single step. Compared with **UPC-613**, all Q_{st} values of **UPC-612** are lower, which assists the regeneration of the adsorbent.

Density Functional Theory (DFT) Calculations

Theoretical simulation is a powerful tool to enable us to unveil the adsorption mechanisms and provide information concerning adsorption sites. To provide the basic insight into the adsorbate-adsorbent interaction, DFT simulations were performed to calculate the stable adsorption configurations and energies of C₂H₂, C₂H₄, and C₂H₆ in **MOF-525**, **MOF-525(Co)**, **UPC-612** and **UPC-613** with the Dmol³ module^[36] from Materials Studio. In view of the size of the task to complete the DFT calculations using a whole MOF unit cell, we used fragmented cluster models cleaved from unit cells representing the actual situations as accurately as possible; the cleaved bonds at cluster boundaries were saturated by protons (Figure 4). The Perdew-Burke-Ernzerhof (PBE) function under the generalized gradient approximation (GGA) was used to complete all-electron spin-unrestricted DFT calculations. DFT-D calculations were performed using Grimme's standard parameters set for the van der Waals correction of gas adsorption. The double numerical basis set including polarization (DNP) was chosen for all atoms. The adsorption energy (ΔE_{ads}) is expressed as $\Delta E_{ads} = E_{ads} + E_{fram} - E_{ads+fram}$, where E_{ads} , E_{fram} and $E_{ads+fram}$ are the total energy of the adsorbate molecule, adsorbent framework, and adsorbate-framework adsorption system, respectively.

The density distributions of the mass centers of C₂H₂, C₂H₄ and C₂H₆ molecules within the structure of **UPC-612** at 298 K and 1 atm were analyzed. It was found that the gas molecules were concentrated mainly at the angle of the cube cage, then at the linker-modified cyclopentadienyl rings. Subsequently, the optimal adsorption sites and adsorption energies of C₂H₂, C₂H₄, and C₂H₆ on **TCP**, **TCP-Co**, **H₄L-L**, and **H₄L-S** linkers and metal clusters were obtained. As shown in Figure 4 a–c, the adsorption sites of C₂H₂, C₂H₄, and C₂H₆ are concentrated in the center of **TCP**, and the corresponding adsorption energies are 26.84, 29.37, and 28.56 kJ mol⁻¹, respectively. In the **TCP-Co** modified with cobalt, the adsorption energies were significantly increased to 54.72, 63.11, and 45.196 kJ mol⁻¹, respectively (Figure 4 d–f). The adsorption energy of C₂H₄ after the modification which placed cobalt in the center of porphyrin reached 63.11 kJ mol⁻¹, which is similar to the chemical adsorption energy and is detrimental to the separation and purification of ethylene. The modified **H₄L-L** and **H₄L-S** showed the same

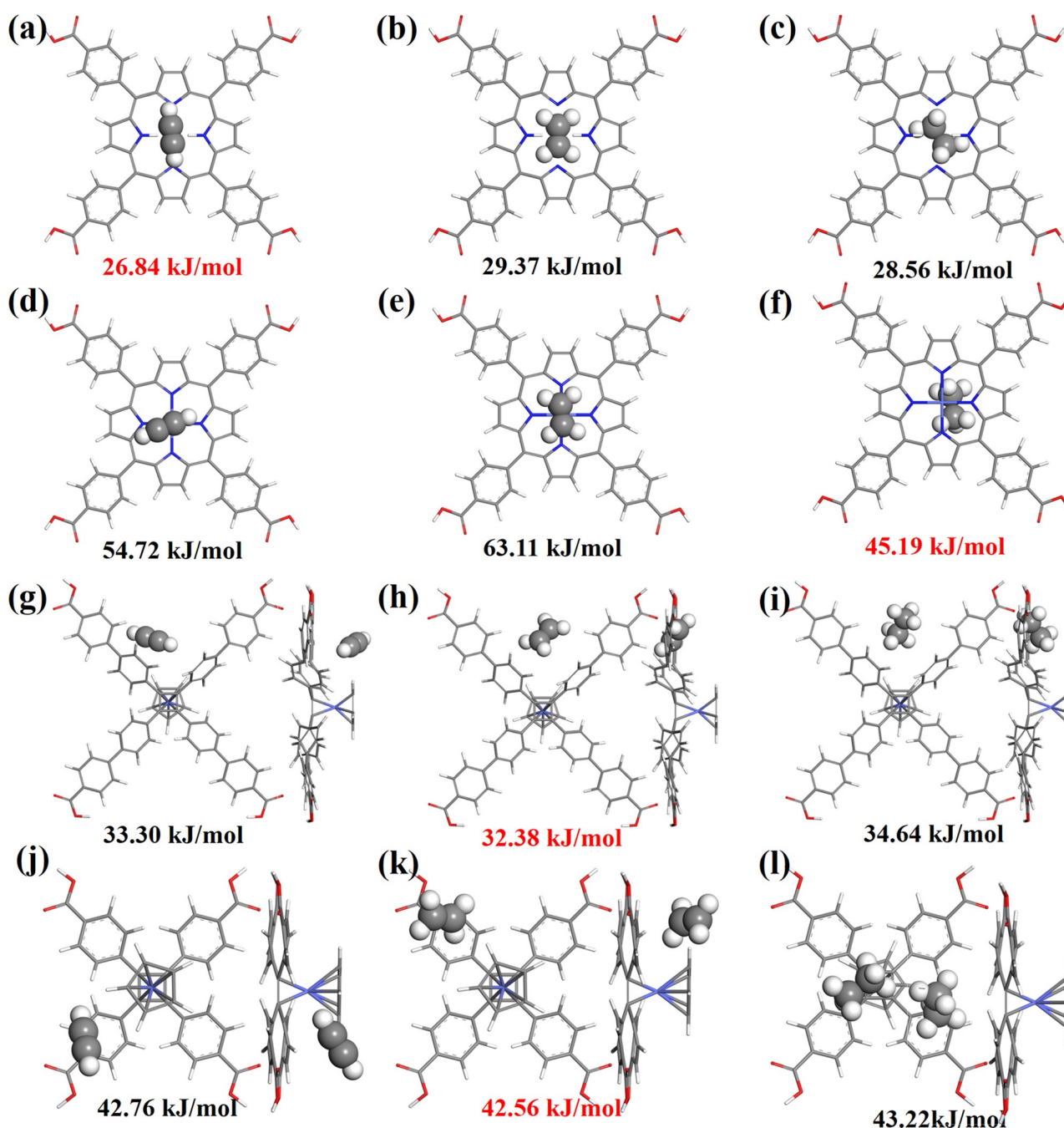


Figure 4. Preferential C₂H₂ (left), C₂H₄ (middle), and C₂H₆ (right), adsorption sites and corresponding adsorption energies in the linker of MOF-525 (a–c), MOF-525(Co) (d–f), UPC-612 (g–i), and UPC-613 (j–l) obtained from first-principles calculations.

tendency for the adsorption of C₂H₂, C₂H₄, and C₂H₆, the adsorption energy of C₂H₄ being the smallest. The adsorption energies of C₂H₂, C₂H₄, and C₂H₆ in **H₄L-L** are 33.3, 32.38, and 34.64 kJ mol⁻¹, and the corresponding adsorption energies in **H₄L-S** are 42.76, 42.56, and 43.22 kJ mol⁻¹, respectively. This follows the same trend as the Q_{st} calculated from the adsorption isotherm and can be attributed to the stronger van der Waals force exerted by the modified cyclopentadiene ring on C₂H₂ and C₂H₆. The adsorption energies of C₂H₂, C₂H₄, and C₂H₆ on the metal clusters are also given, as shown in Figure 5 and S29, and are generally greater than those on

linkers. It is also normal that the unsaturated coordination sites on the metal clusters provide an increased weak interaction for the gas. It should be noted that the adsorption energy of C₂H₄ for Zr₆-Clusters is less than that of C₂H₂ and C₂H₆ in **UPC-612**, but higher in **MOF-525** and **MOF-525(Co)**. This indicates that the electron cloud and space effect of linkers affect the adsorption sites of the zirconium clusters. It was proved theoretically that the new modification method provides the possibility for the material useful for the purification of ethylene.

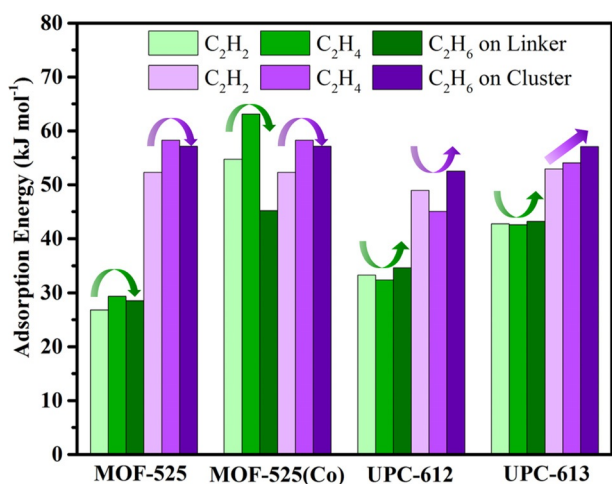


Figure 5. Adsorption energies of C_2H_2 , C_2H_4 , and C_2H_6 on linker and metal cluster.

Breakthrough Experiments

To evaluate the effect of gas selectivity, breakthrough experiments were performed in a typical process (Scheme S3). The breakthrough experiments were performed on **MOF-525**, **MOF-525(Co)**, **UPC-612** and **UPC-613**, with C_2H_6/C_2H_4 (10/90, 50/50), C_2H_2/C_2H_4 (10/90, 50/50), and C_2H_6/C_2H_2 (1/1/1) mixtures flowed over a packed bed at a total flow rate of 2 mL min^{-1} at 298 K (Figure 6 and Table S7,8). With C_2H_6/C_2H_4 (50/50) as an example, C_2H_4 was first to elute through the bed, before it was contaminated with undetectable amounts of C_2H_6 , resulting in a high concentration of C_2H_4 feed with a purity of $\geq 99.99\%$. After a period of time, C_2H_6 broke through after the adsorbent became saturated, and then the outlet gas stream quickly reached equimolar concentrations. Replacing the gas with C_2H_6/C_2H_4 (10/90), C_2H_2/C_2H_4 (50/50), and C_2H_2/C_2H_4 (10/90) led to similar results, and the difference between them lies in the separation time. To make the systematic comparison for the C_2H_4 separation performance in the selected MOFs, C_2H_4 purity and productivity were calculated from their breakthrough curves (Table S8). For **UPC-612**, 0.56 mmol g^{-1} of C_2H_4 with $\geq 99.99\%$ purity can be recovered from the C_2H_4/C_2H_6 (50/50) mixture in a single breakthrough operation; this value is nearly three times that for the benchmark material **MAF-49** (0.28 mmol g^{-1}),^[37] and slightly lower than for **Fe₂(O₂)(dobdc)** (0.79 mmol g^{-1}).^[10] The productivity of **UPC-612** is nearly ten times that of **MOF-525** (0.05 mmol g^{-1}) and **MOF-525(Co)** (0.07 mmol g^{-1}), which have the same structure platform. However, the separation performance of **UPC-613** (0.47 mmol g^{-1}) with the same modification group did not change with the cage size, and the productivity was similar to that of **UPC-612**. **UPC-612** also showed excellent performance in the separation of C_2H_2/C_2H_4 (50/50), the recovery

C_2H_4/C_2H_2 (1/1/1) mixtures flowed over a packed bed at a total flow rate of 2 mL min^{-1} at 298 K (Figure 6 and Table S7,8). With C_2H_6/C_2H_4 (50/50) as an example, C_2H_4 was first to elute through the bed, before it was contaminated with undetectable amounts of C_2H_6 , resulting in a high concentration of C_2H_4 feed with a purity of $\geq 99.99\%$. After a period of time, C_2H_6 broke through after the adsorbent became saturated, and then the outlet gas stream quickly reached equimolar concentrations. Replacing the gas with C_2H_6/C_2H_4 (10/90), C_2H_2/C_2H_4 (50/50), and C_2H_2/C_2H_4 (10/90) led to similar results, and the difference between them lies in the separation time. To make the systematic comparison for the C_2H_4 separation performance in the selected MOFs, C_2H_4 purity and productivity were calculated from their breakthrough curves (Table S8). For **UPC-612**, 0.56 mmol g^{-1} of C_2H_4 with $\geq 99.99\%$ purity can be recovered from the C_2H_4/C_2H_6 (50/50) mixture in a single breakthrough operation; this value is nearly three times that for the benchmark material **MAF-49** (0.28 mmol g^{-1}),^[37] and slightly lower than for **Fe₂(O₂)(dobdc)** (0.79 mmol g^{-1}).^[10] The productivity of **UPC-612** is nearly ten times that of **MOF-525** (0.05 mmol g^{-1}) and **MOF-525(Co)** (0.07 mmol g^{-1}), which have the same structure platform. However, the separation performance of **UPC-613** (0.47 mmol g^{-1}) with the same modification group did not change with the cage size, and the productivity was similar to that of **UPC-612**. **UPC-612** also showed excellent performance in the separation of C_2H_2/C_2H_4 (50/50), the recovery

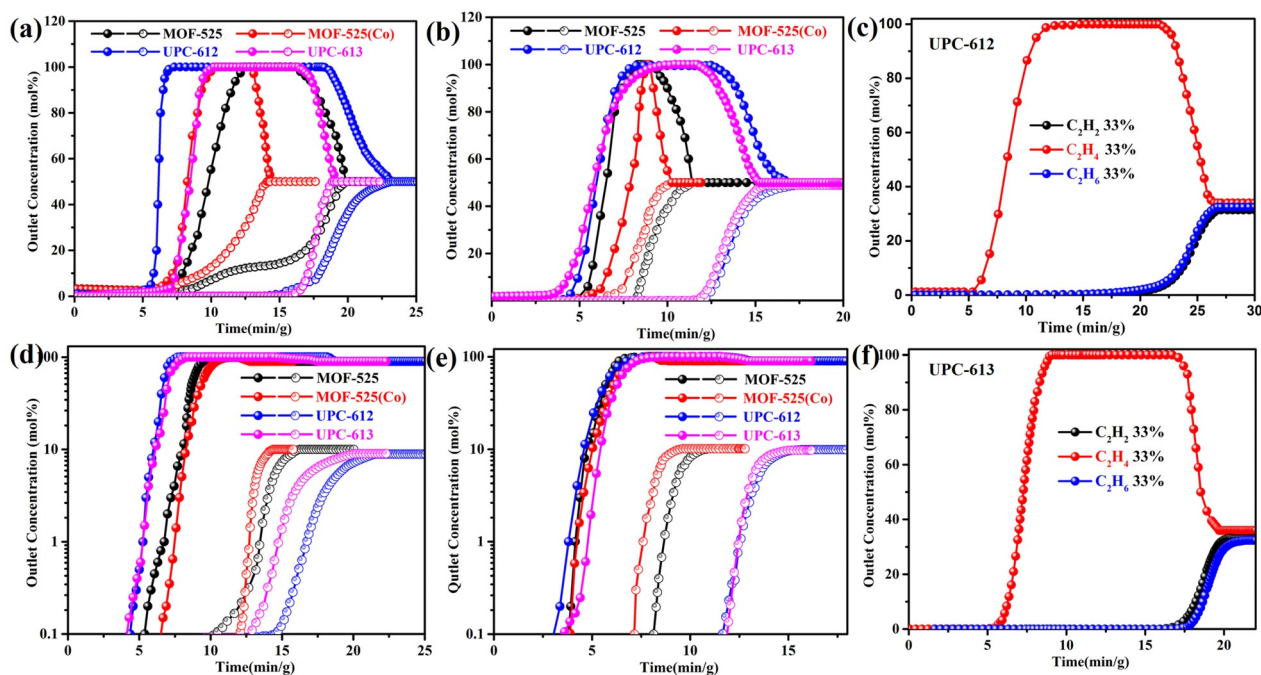


Figure 6. Breakthrough experiments. a) Experimental column breakthrough curves for C_2H_6/C_2H_4 (50/50) mixtures absorber bed packed with **MOF-525**, **MOF-525(Co)**, **UPC-612**, and **UPC-613**, respectively; b) Experimental column breakthrough curves for C_2H_2/C_2H_4 (50/50) mixtures absorber bed packed with **MOF-525**, **MOF-525(Co)**, **UPC-612**, and **UPC-613**, respectively; c) Experimental column breakthrough curves for $C_2H_6/C_2H_4/C_2H_2$ (33/33/33) mixtures and an absorber bed packed with **UPC-612**; d) Experimental column breakthrough curves for C_2H_6/C_2H_4 (10/90) mixtures absorber bed packed with **MOF-525**, **MOF-525(Co)**, **UPC-612**, and **UPC-613**, respectively; e) Experimental column breakthrough curves for C_2H_2/C_2H_4 (10/90) mixtures absorber bed packed with **MOF-525**, **MOF-525(Co)**, **UPC-612**, and **UPC-613**, respectively; f) Experimental column breakthrough curves for $C_2H_6/C_2H_4/C_2H_2$ (33/33/33) mixtures absorber bed packed with **UPC-613**. (Description: In (a) and (d), all filled spheres represent ethylene and all open spheres represent ethane; in (b) and (e), all filled spheres represent ethylene and all open spheres represent acetylene.)

value (0.35 mmol g^{-1}) is nearly twice that for **MOF-525** (0.15 mmol g^{-1}), six times that for **MOF-525(Co)** (0.06 mmol g^{-1}), and similar to **UPC-613** (0.38 mmol g^{-1}). **UPC-612** has the highest separation potential for recovering the pure C_2H_4 from $\text{C}_2\text{H}_6/\text{C}_2\text{H}_4$ (50/50) and $\text{C}_2\text{H}_2/\text{C}_2\text{H}_4$ (50/50) mixtures during the adsorption process (Figure 6a and b). Even when the concentrations of C_2H_6 and C_2H_2 decrease to 10% (Figure 6d and e), **UPC-612** maintains the highest separation potential (Table S8), which makes it the most promising material for the separation of C_2H_4 from $\text{C}_2\text{H}_6/\text{C}_2\text{H}_4$ and $\text{C}_2\text{H}_2/\text{C}_2\text{H}_4$ mixtures. These excellent breakthrough results encouraged us to further evaluate the separation performance of ternary gas mixtures closer to industrial applications, and to expand the gas ratio to 1/1/1 for $\text{C}_2\text{H}_2/\text{C}_2\text{H}_4/\text{C}_2\text{H}_6$. As shown in Figure 6c, C_2H_2 , C_2H_4 , and C_2H_6 are simultaneously adsorbed in **UPC-612**. After a period of time, C_2H_4 first breaks through the adsorbent to produce pure C_2H_4 , then the adsorbent reaches saturation, and C_2H_2 and C_2H_6 breakthrough at the same time. The separation time was 16 min g^{-1} , and the productivity was calculated to be 0.47 mmol g^{-1} . This is the first case of a single adsorbent for one-step C_2H_4 purification from a large proportion (1/1/1) ternary mixture of $\text{C}_2\text{H}_2/\text{C}_2\text{H}_4/\text{C}_2\text{H}_6$. The cycling and regeneration capabilities of **UPC-612** were further studied by breakthrough cycle experiments (Figure S30), which showed no noticeable decrease in the mean residence times for both C_2H_4 , C_2H_6 and C_2H_2 within five continuous cycles under ambient conditions. The **UPC-612** material retained its stability after the breakthrough cycling test (Figure S32). The same experiment was carried out on **UPC-613**, and the similar results obtained confirmed the feasibility of this new modification method. Therefore, it is a good choice for functional modification and selective separation of mixed gases.

Conclusion

In conclusion, we have discovered and are reporting a new modification method for C_2H_4 purification. Cyclopentadiene cobalt was introduced to an open *ftw* platform to obtain **UPC-612** and **UPC-613** with different cage sizes. These can purify C_2H_4 not only from $\text{C}_2\text{H}_4/\text{C}_2\text{H}_6$ (50/50), but also from $\text{C}_2\text{H}_4/\text{C}_2\text{H}_2$ (50/50) and they can abstract C_2H_4 from a $\text{C}_2\text{H}_2/\text{C}_2\text{H}_4/\text{C}_2\text{H}_6$ (1/1/1) ternary mixture. This is the first time that a single adsorbent has been used to directly produce polymer grade ethylene in one step from a large ternary mixture of gases. Theoretical calculations show that the introduction of cyclopentadienyl units enhances the interactions of the framework with C_2H_2 and C_2H_6 , which are preferentially adsorbed from the mixture of gases instead of C_2H_4 . This material can readily produce $\geq 99.99\%$ pure C_2H_4 from $\text{C}_2\text{H}_2/\text{C}_2\text{H}_4/\text{C}_2\text{H}_6$ mixtures during the first breakthrough cycle with moderately high productivity and a low energy cost. The modification method we developed in this work may facilitate extensive research on the practically functional porous materials for cheap and efficiently important industrial separation.

Acknowledgements

This work was financially supported by the National Natural Science Foundation of China (NSFC Grant Nos. 21875285), Taishan Scholar Foundation (ts201511019). Key Research and Development Projects of Shandong Province (2019JZZY010331), Fundamental Research Funds for the Central Universities(20CX05010A).

Conflict of interest

The authors declare no conflict of interest.

Keywords: cobalt · ethylene purification · metal-organic frameworks (MOFs) · one-step purification · ternary gas mixture

- [1] S. Chu, Y. Cui, N. Liu, *Nat. Mater.* **2017**, *16*, 16–22.
- [2] A. M. Robert, *Handbook of Petrochemicals Production Processes*, McGraw-Hill Education, New York, **2005**.
- [3] T. Ren, M. Patel, K. Blok, *Energy* **2006**, *31*, 425–451.
- [4] Y. Zhang, J.-h. Wu, D.-k. Zhang, *Energy Fuels* **2008**, *22*, 1142–1147.
- [5] K. Adil, Y. Belmabkhout, R. S. Pillai, A. Cadiau, P. M. Bhatt, A. H. Assen, G. Maurin, M. Eddaoudi, *Chem. Soc. Rev.* **2017**, *46*, 3402–3430.
- [6] Z. Bao, G. Chang, H. Xing, R. Krishna, Q. Ren, B. Chen, *Energy Environ. Sci.* **2016**, *9*, 3612–3641.
- [7] J. Y. Lin, *Science* **2016**, *353*, 121–122.
- [8] Q. G. Zhai, X. Bu, C. Mao, X. Zhao, L. Daemen, Y. Cheng, A. J. Ramirez-Cuesta, P. Feng, *Nat. Commun.* **2016**, *7*, 13645.
- [9] S. M. Sadrameli, *Fuel* **2016**, *173*, 285–297.
- [10] D. S. Sholl, R. P. Lively, *Nature* **2016**, *532*, 435–437.
- [11] P. J. Bereciartua, A. Cantin, A. Corma, J. L. Jorda, M. Palomino, F. Rey, S. Valencia, E. W. Corcoran, Jr., P. Kortunov, P. I. Ravikovitch, A. Burton, C. Yoon, Y. Wang, C. Paur, J. Guzman, A. R. Bishop, G. L. Casty, *Science* **2017**, *358*, 1068–1071.
- [12] A. Cadiau, K. Adil, P. M. Bhatt, Y. Belmabkhout, M. Eddaoudi, *Science* **2016**, *353*, 137–140.
- [13] C. Gu, N. Hosono, J. J. Zheng, Y. Sato, S. Kusaka, S. Sakaki, S. Kitagawa, *Science* **2019**, *363*, 387–391.
- [14] B. Li, X. Cui, D. O’Nolan, H. M. Wen, M. Jiang, R. Krishna, H. Wu, R. B. Lin, Y. S. Chen, D. Yuan, H. Xing, W. Zhou, Q. Ren, G. Qian, M. J. Zaworotko, B. Chen, *Adv. Mater.* **2017**, *29*, 1704210.
- [15] P. Q. Liao, N. Y. Huang, W. X. Zhang, J. P. Zhang, X. M. Chen, *Science* **2017**, *356*, 1193–1196.
- [16] R. B. Lin, L. Li, H. L. Zhou, H. Wu, C. He, S. Li, R. Krishna, J. Li, W. Zhou, B. Chen, *Nat. Mater.* **2018**, *17*, 1128–1133.
- [17] E. D. Bloch, W. L. Queen, R. Krishna, J. M. Zadrozny, C. M. Brown, J. R. Long, *Science* **2012**, *335*, 1606–1610.
- [18] L. Li, R. B. Lin, R. Krishna, H. Li, S. Xiang, H. Wu, J. Li, W. Zhou, B. Chen, *Science* **2018**, *362*, 443–446.
- [19] X. Cui, K. Chen, H. Xing, Q. Yang, R. Krishna, Z. Bao, H. Wu, W. Zhou, X. Dong, Y. Han, B. Li, Q. Ren, M. J. Zaworotko, B. Chen, *Science* **2016**, *353*, 141–144.
- [20] K. J. Chen, D. G. Madden, S. Mukherjee, T. Pham, K. A. Forrest, A. Kumar, B. Space, J. Kong, Q. Y. Zhang, M. J. Zaworotko, *Science* **2019**, *366*, 241–246.
- [21] H. G. Hao, Y. F. Zhao, D. M. Chen, J. M. Yu, K. Tan, S. Ma, Y. Chabal, Z. M. Zhang, J. M. Dou, Z. H. Xiao, G. Day, H. C. Zhou, T. B. Lu, *Angew. Chem. Int. Ed.* **2018**, *57*, 16067–16071; *Angew. Chem.* **2018**, *130*, 16299–16303.

- [22] Y. Bai, Y. B. Dou, L. H. Xie, W. Rutledge, J. R. Li, H. C. Zhou, *Chem. Soc. Rev.* **2016**, *45*, 2327–2367.
- [23] S. Kitagawa, *Angew. Chem. Int. Ed.* **2015**, *54*, 10686–10687; *Angew. Chem.* **2015**, *127*, 10834–10835.
- [24] H. Zeng, X. J. Xie, M. Xie, Y. L. Huang, D. Luo, T. Wang, Y. Zhao, W. Lu, D. Li, *J. Am. Chem. Soc.* **2019**, *141*, 20390–20396.
- [25] W. Morris, B. Voloskiy, S. Demir, F. Gandara, P. L. McGrier, H. Furukawa, D. Cascio, J. F. Stoddart, O. M. Yaghi, *Inorg. Chem.* **2012**, *51*, 6443–6445.
- [26] S. Yuan, L. Feng, K. Wang, J. Pang, M. Bosch, C. Lollar, Y. Sun, J. Qin, X. Yang, P. Zhang, Q. Wang, L. Zou, Y. Zhang, L. Zhang, Y. Fang, J. Li, H. C. Zhou, *Adv. Mater.* **2018**, *30*, 1704303.
- [27] S. Sen, N. Hosono, J. J. Zheng, S. Kusaka, R. Matsuda, S. Sakaki, S. Kitagawa, *J. Am. Chem. Soc.* **2017**, *139*, 18313–18321.
- [28] H. Zeng, M. Xie, Y. L. Huang, Y. Zhao, X. J. Xie, J. P. Bai, M. Y. Wan, R. Krishna, W. Lu, D. Li, *Angew. Chem. Int. Ed.* **2019**, *58*, 8515–8519; *Angew. Chem.* **2019**, *131*, 8603–8607.
- [29] L. Jiao, W. Yang, G. Wan, R. Zhang, X. Zheng, H. Zhou, S. H. Yu, H. L. Jiang, *Angew. Chem. Int. Ed.* **2020**, *59*, 20589–20595; *Angew. Chem.* **2020**, *132*, 20770–20776.
- [30] A. Luna-Triguero, J. M. Vicent-Luna, R. M. Madero-Castro, P. Gomez-Alvarez, S. Calero, *ACS Appl. Mater. Interfaces* **2019**, *11*, 31499–31507.
- [31] W. Fan, X. Wang, X. Zhang, X. Liu, Y. Wang, Z. Kang, F. Dai, B. Xu, R. Wang, D. Sun, *ACS Cent. Sci.* **2019**, *5*, 1261–1268.
- [32] R. B. Lin, H. Wu, L. Li, X. L. Tang, Z. Li, J. Gao, H. Cui, W. Zhou, B. Chen, *J. Am. Chem. Soc.* **2018**, *140*, 12940–12946.
- [33] S. Yang, A. J. Ramirez-Cuesta, R. Newby, V. Garcia-Sakai, P. Manuel, S. K. Callear, S. I. Campbell, C. C. Tang, M. Schroder, *Nat. Chem.* **2015**, *7*, 121–129.
- [34] H. Deng, C. J. Doonan, H. Furukawa, R. B. Ferreira, J. Towne, C. B. Knobler, B. Wang, O. M. Yaghi, *Science* **2010**, *327*, 846–850.
- [35] H. Furukawa, K. E. Cordova, M. O’Keeffe, O. M. Yaghi, *Science* **2013**, *341*, 1230444.
- [36] S. Grimme, J. Antony, S. Ehrlich, H. Krieg, *J. Chem. Phys.* **2010**, *132*, 154104.
- [37] P. Q. Liao, W. X. Zhang, J. P. Zhang, X. M. Chen, *Nat. Commun.* **2015**, *6*, 8697.

Manuscript received: January 18, 2021

Accepted manuscript online: March 4, 2021

Version of record online: March 30, 2021